JLAB-TN-17-029

May 17, 2017

Experience with the fabrication, processing and testing of the prototype "C75" 5-cell cavities

G. Ciovati, A. Anderson, W. Clemens, D. Combs, K. Davis, J. Dail, C. Dreyfuss, J. Follkie, D. Forehand, J. Guo, T. Harris, J. Henry, C. Johnson, R. Martin, F. Marhauser, G. R. Myneni, R. Overton, R. Rimmer, T. Sessoms, L. Turlington, S. Williams, A. Wildeson, C. Wilson

Abstract

Three 5-cell prototype cavities have been fabricated, processed and tested as part of an R&D program aiming at providing cavities to be installed during the refurbishment of some of the original CEBAF cryomodules in order to reach an energy gain of 75 MeV per cyromodule ("C75"). The experience with the fabrication, processing and testing of these cavities is reported in this technical note. The two best cavities, 5C75-003 and 5C75-001 were assembled into a "pair" to be installed in the cryomodule C50-7B and achieved an accelerating gradient of 13.7 MV/m and 19.3 MV/m, respectively with a quality factor greater than 8×10^9 at 2.07 K.

1. Introduction

In order to improve the energy gain of refurbished original CEBAF cryomodules with minimal cost, it was proposed to replace the cavity cells with newer ones of a new shape and material, which would allow achieving both higher accelerating gradient and quality factor than the original cavities. The end groups would be cut from existing cavities and welded to the new multi-cell structure to save as much of the existing cavity components as practically possible. The cell shape was chosen to be identical with the 'high current' shape designed for a 1 A-class FEL at JLab [1]. The material was chosen to be ingot Nb, a cavity material technology pioneered at Jefferson Lab in 2004. The performance specification is an accelerating gradient, E_{acc}, of 18.7 MV/m with a quality factor, Q_0, greater than 8×10^9 at 2.07 K. Three prototype cavities were built and the two with the best RF performance were assembled into a cavity pair to be installed in the next refurbished cryomodule, which is planned to be installed in CEBAF in summer 2017.

2. Cavity Material

Two Nb ingots produced by CBMM, Brazil, as part of a company's R&D program and given to Jefferson Lab for evaluation and testing were used for the fabrication of cavities 5C75-001 and 5C75-002. A center hole was cut by wire electro-discharge machining and the ingots were sliced into 1/8" thick discs with a multi-wire slicing machine at Slicing Tech in Pennsylvania. The thickness tolerance achieved was ±0.004" and the average surface roughness was better than 63 μin. Additional ingot Nb

discs to build 5C75-003 were purchased from Tokyo-Denkai, Japan. Table I summarizes the material and its properties for each cavity. Since the initial developments in 2004, ingot Nb technology has demonstrated to be an excellent alternative to standard fine-grain Nb [2], and the use of a material with lower residual resistivity ratio (RRR) can be advantageous to achieve a higher quality factor, which is very beneficial for CW accelerators [3]. Medium purity (RRR = 100 – 200) ingot Nb material is an ideal combination to achieve good performance at lower cost than standard fine-grain, high-purity (RRR > 250) Nb. Pictures of the ingots and of a disc, after 5 μm buffered chemical polishing (BCP) are shown in Fig. 1.

Table I. Materials used for the fabrication of the three prototype cavities.

Cavity	**Ingot SN**	**Supplier**	**RRR**	**Ta content (wt. ppm)**
5C75-001	2370-5	CBMM, Brazil	118	1350
5C75-002	2667-5	CBMM, Brazil	114	670
5C75-003	NC-1654	Tokyo-Denkai, Japan	496	29

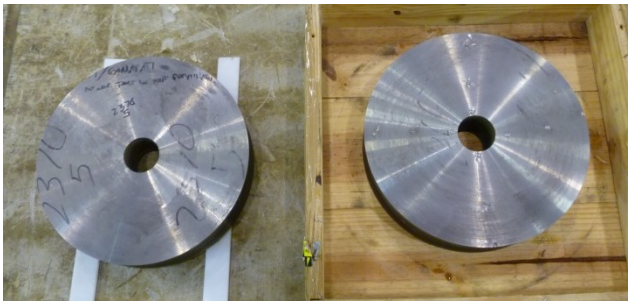

(a)

(b)

Figure 1. Picture of the CBMM Nb ingots (a) and of a disc cut from the ingots after light chemical etch (b).

Several single-cell cavities were fabricated, processed and tested in order to check that the quality of the material allows achieving the required cavity performance. This was done as part of a broader R&D effort to evaluate the performance of ingot Nb cavities [3]. The results showed that buffered chemical polishing had a tendency to produce etch pits on the surface of medium and lower purity ingot Nb material and that centrifugal barrel polishing (CBP) followed by electropolishing (EP) were processing techniques better suited to achieve higher accelerating gradient with this type of material. On the other hand, E_{acc} > 30 MV/m was easily achieved with high-purity ingot Nb cavities treated by BCP [4]. Figure 2 shows a plot of the Q_0 as a function of peak surface magnetic field, B_p, measured on single-cell cavities made from the same material used to fabricate the C75 prototype cavities. The processing sequence prior to the RF test is listed in Table II.

Table II. Treatment sequence of single-cell cavities to qualify the material used for the C75 5-cell cavities. The results from the RF tests of the cavities are shown in Fig. 2.

Cavity	f (GHz)	Ingot SN	Supplier	RRR	Treatments prior to RF test
F3F4	1.5	2370-5	CBMM, Brazil	118	100 μm CBP, 50 μm BCP, 800 °C/2 h, 20 μm BCP, 120 °C/12 h, HF rinse, 30 μm EP, 120 °C/12 h
C75-SC1	1.5	2667-5	CBMM, Brazil	114	60 μm CBP, 30 μm EP, 800 °C/3 h, 30 μm EP
TD2	1.3	n/a	Tokyo-Denkai, Japan	> 300	90 μm BCP, 600 °C/10 h, 60 μm BCP, 120 °C/20 h

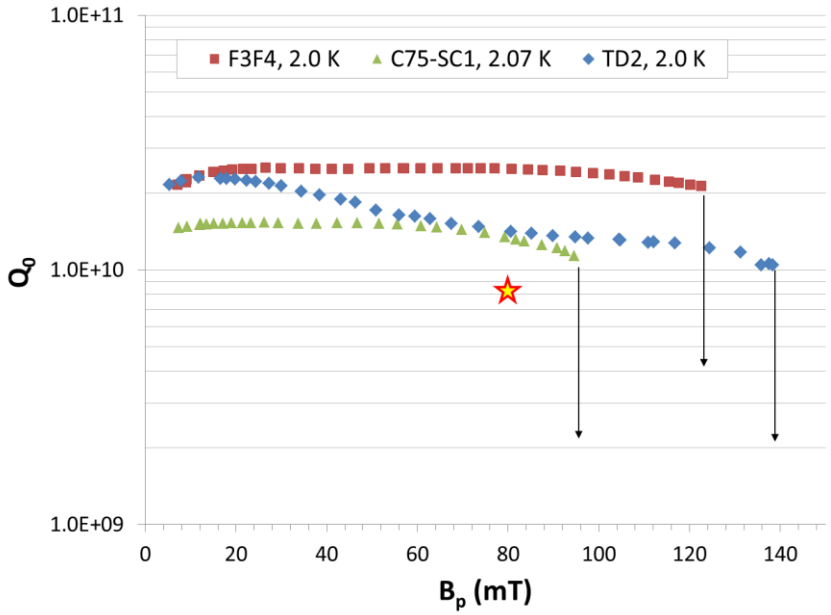

Figure 2. Examples of the RF performance achieved in single-cell cavities built from the material used for the C75 prototype cavities. The "star" symbol is the performance specification for the C75 cavities.

3. Cavity Fabrication

A drawing of the cavity is shown in Fig. 3. The discs were pressed into half-cells (items 1 and 3 in Fig. 3) with the standard deep-drawing method, using Aluminum dies and a 150 ton press. Whereas 5W30 motor oil was used in the past as a lubricant for both dies and Nb discs, a different lubricant (ICC 1599, International Chemical Co, 50% diluted) was qualified to be used for deep-drawing of Nb cells, aiming at reducing potential hydrocarbon contamination of the material. Another advantage is that ICC 1599 is fully water soluble, so it is easy to clean off the residue after deep drawing. After deep-drawing and coining of the iris, the half-cells were subjected to a light chemical etch (~10 μm removal) by BCP, followed by vacuum annealing at 800 °C/2 h. The half-cells were then stamped and coined once more in

order to mitigate spring-back effects and to achieve a shape closest to the design. A picture of a set of half-cells after stamping is shown in Fig. 4. A 3D color plot of the deviation of the shape of a half-cell from the shape of the die, shown in Fig. 5, indicate that the equator has more of an oval, rather than round shape. This measurement was done during an on-site demonstration of the ROMER 7525SI portable CMM scanner.

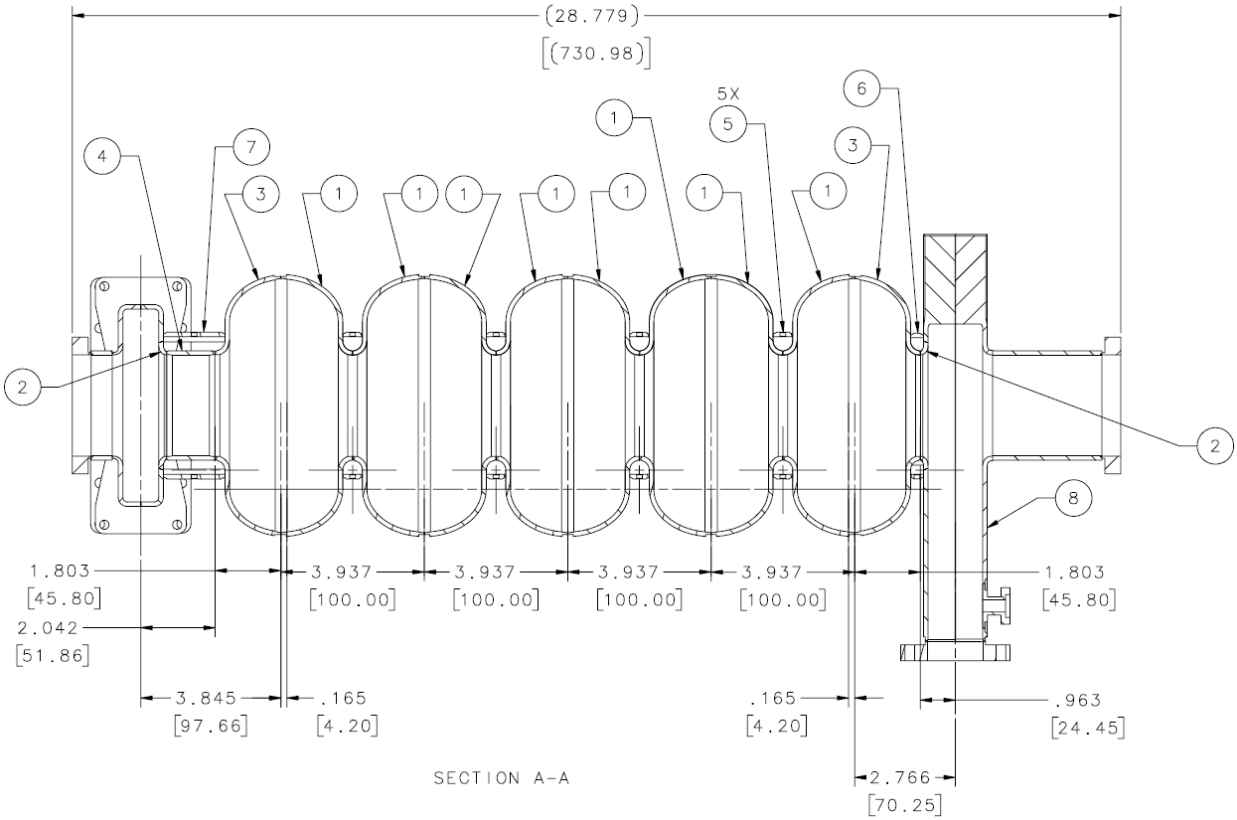

Figure 3. Drawing of the C75 cavity. Dimensions are in inches [mm].

Figure 4. Set of half-cells used to fabricate 5C75-001 after stamping.

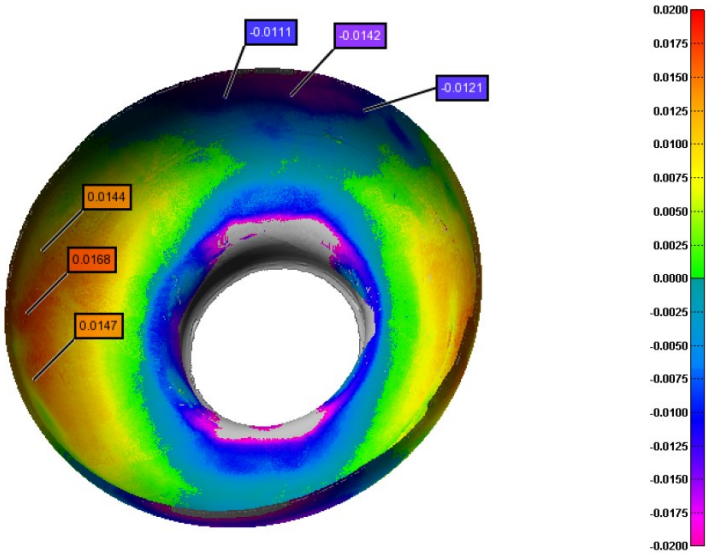

Figure 5. 3D plot of the point-to-point deviation of a C75 Nb half-cell from the die shape. Dimensions are in inches.

The extra material at both iris and equator of the half-cells after deep-drawing was cut by wire-EDM, leaving an additional length of 0.1" at both iris and equator for the final trimming. Using wire-EDM instead of milling was far less time consuming and resulted in better flatness of the surfaces. The iris of each half-cell was placed in a holding fixture, machined to a length 0.009" beyond the reference line and with 1/16" thick welds prep by milling. The frequencies and Qs of the TM_{010}-π mode of each half-cell with a tube contacting the iris were measured with an RF testing fixture developed for C100 prototype cavities. Q-values above 3000 were typically achieved, which implies sufficiently good RF contact between a half cell and the RF fixture. The equator inner diameter and its roundness were measured with a CMM machine. Plots of the measured frequency, equator inner diameter and roundness of all the half-cells used for the three prototype cavities are shown in Fig. 6.

The half-cells for the center section of the cavities were degreased, the iris region etched by BCP 1:1:1 to remove ~20 μm, rinsed with DI water, dried and placed in a sealed bag. Irises of pair of half-cells were welded from inside and outside by electron-beam welding, producing dumb-bells. Measurements of the length of half-cells and of corresponding dumb-bells consistently showed a weld-shrinkage of ~0.040", more than twice the expected value. The cause for this is unclear, however the additional length left at the iris of the half-cells was changed to 0.015" for the set to be used for 5C75-003 in order to compensate for the larger weld shrinkage.

Niobium stiffening rings (items 5 in Fig. 3) were machined to a custom length for each dumb-bell, etched by BCP to remove ~10 μm, hold into position by set screws and electron beam (EB) welded to each dumb-bell. The equators on both sides of six dumbbells were trimmed by the same amount in a holding fixture by milling and subsequent measurements of the change in frequency and length were made in order to determine the trimming coefficient, df/dz = (-143 ± 5) MHz/in. The trimming coefficient from electromagnetic simulation with SUPERFISH was -126 MHz/in.

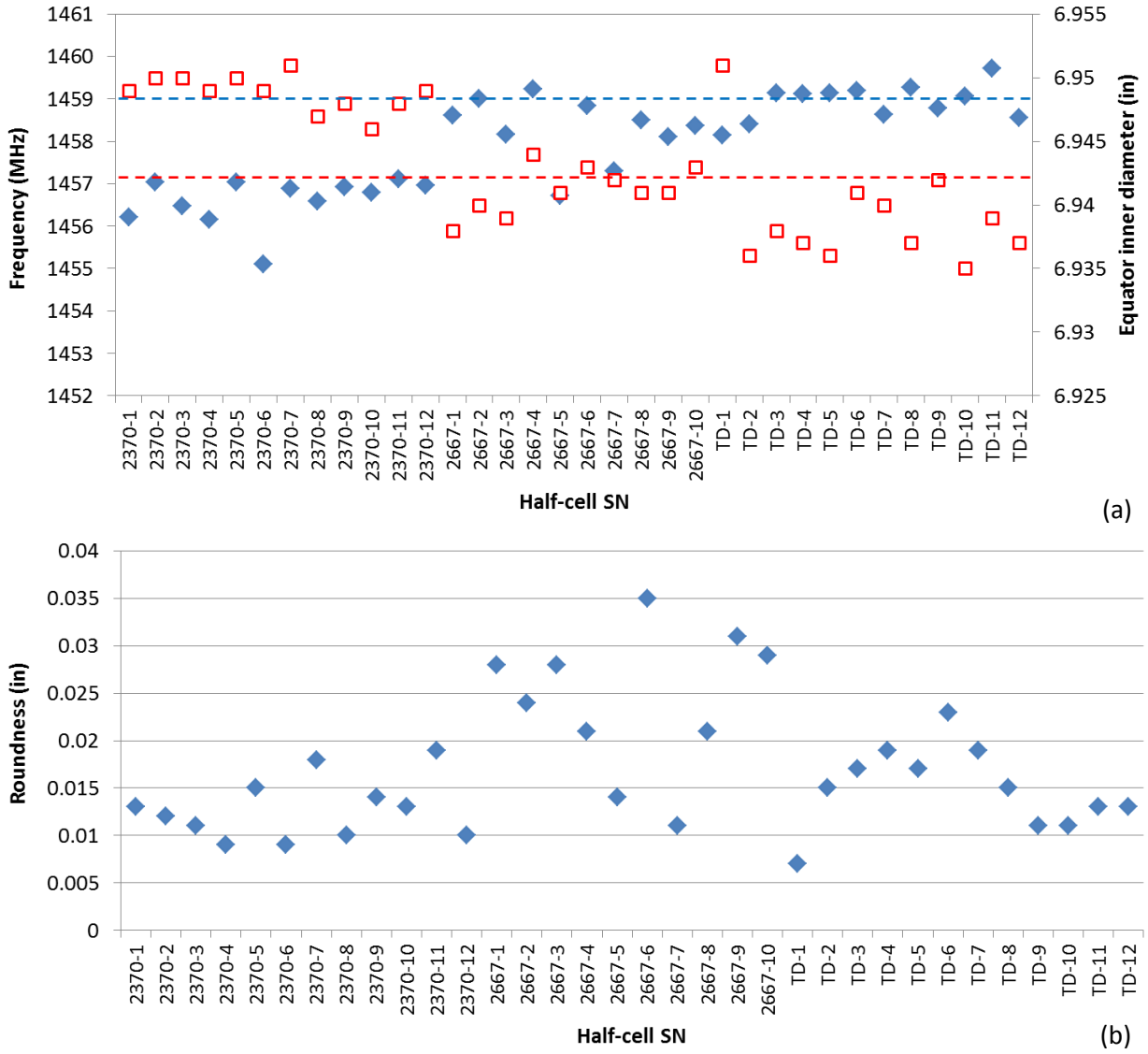

Figure 6. (a) Equator inner diameter (empty square symbols) and frequency (solid diamond symbols) and roundness (b) for all the half-cells made for the C75 cavities. Dashed lines represent target values.

The material qualification study indicated that CBP and EP results in better performance than BCP for medium and low-purity ingot Nb cavities, however the CBP machine at JLab does not have large enough barrels to accommodate the fundamental power coupler (FPC) and higher-order modes (HOM) end-groups of a 5-cell cavity. Therefore it was decided to weld straight beam tubes to cavities 5C75-001 and 5C75-002, to allow for CBP.

The end half-cells (item 3 in Fig. 3) for cavities 5C75-001 and 5C75-002 were trimmed at the iris and equator to achieve the target frequency and 1/16" thick weld prep was machined by milling. The irises were then EB welded by full penetration from the outside to straight beam tubes. End-groups from three spare cavities were cut by wire-EDM and two Nb adapter rings (item 2 in Fig. 3) were machined to interface between the end-groups and the end-cells. The machined regions of the end-groups and the

adapter rings were etched by BCP to remove ~10 μm and the adapter rings were EB welded to the end groups. The iris of the end-cell at the HOM-side for 5C75-003 was EB welded from the inside and outside to the adapter ring and three stiffening ring sections (item 6 in Fig. 3) were EB welded between the HOM waveguide wall and the wall of the end half-cell. A short Nb tube (item 4 in Fig, 3) was EB welded from the outside to the iris of the other end half-cell and the FPC end-group with adapter ring was then EB welded to the tube's end. The length of the tube between the end-cell and the FPC was optimized to achieve a Q_{ext} of 2×10^7. Two stiffening ring sections (item 7 in Fig. 3) were EB welded between the FPC waveguide wall and the wall of the end half-cell. The location of the stiffening rings is at a 48 mm radius from the cells' axis in order for the C75 cavities to have the same stiffness as the original CEBAF cavities, as determined by finite-element analysis and verified experimentally [5].

Each side of the dumb-bells was placed in the trimming fixture and pressed with 10 kpsi to compensate for deviations of the shape after welding the stiffening rings. Each side of each dumb-bell was placed in the trimming fixture and the equators were trimmed by milling to a length determined from the RF measurements to achieve the target frequency, with an additional 0.009" to compensate for weld shrinkage. 1/16" thick weld prep was machined by milling. It should be noted that an undercut is machined at the equator as part of the weld-prep machining to achieve the same diameter for all dumb-bells, and it results in a decrease of frequency by ~1 MHz. A detail of the equator weld-prep is shown in Fig. 6. The target frequencies for the C75 5-cell cavity after fabrication and of its subcomponents are listed in Table III. The inner surface of the dumb-bells and end-cells were lightly hand-polished with a grinding tool and aluminum oxide abrasive discs to remove any visible scratches and dints and to smoothen some of the grain boundary areas.

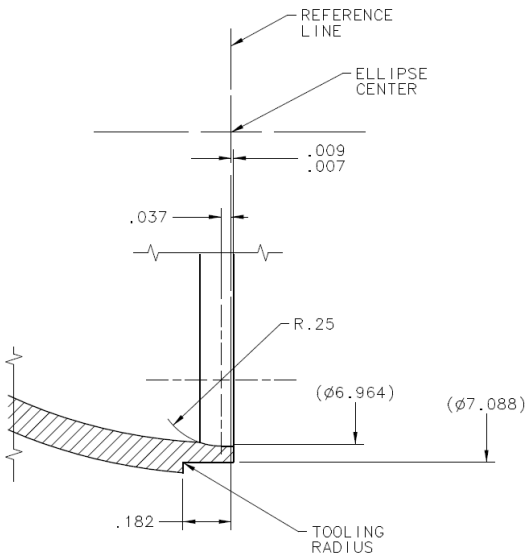

Figure 7. Detail of the equator weld-prep. 0.009" additional length was estimated for weld shrinkage and an undercut was specified to obtain a uniform diameter in the weld area. Dimensions are in inches.

Table III. Room temperature TM010 π-mode target frequencies for dumb-bells and end half-cells, prior to equatorial EB welding, and for a competed cavity.

Component	Frequency (MHz)
Dumb-bell	1494.283
End half-cell with end group	1493.518
5-cell cavity	1495.572

One of the most critical steps on the fabrication of an SRF cavity is the EB welding of the equators of the cells because any defect or contamination in this region, where the surface magnetic field is highest, can result in a reduced quench field. Past experience with fabrication, processing and testing of multi-cell cavities made of ingot Nb at Jefferson Lab indicated that the average quench field of such cavities was 40% lower than that of similar single-cell cavities made from the same material and that a blow-through hole occurred in at least one of the equatorial EB welds of each multi-cell cavity, which needed to be repaired [6].

In order to improve the reliability of the EB welding, an improved protocol for parts cleaning and assembly was adopted, for which the equator region to be welded is etched to remove ~30 μm instead of ~10 μm, the parts were ultrasonically cleaned in DI water after etching, dried and bagged [7]. The stack up of parts to be welded was done under a laminar flow tent inside the EBW room. Another change that was implemented for EB welding of the three prototype cavities for the C75 project was to do inside/outside equator welds rather than full-penetration welds, except for the last equator weld between two cavity halves, as it was successfully implemented at KEK. This arrangement should result in a smoother underbead and much lower risk of a blow-through hole. A non-chlorinated, sulfur-free machining coolant (Syntilo 9918, Castrol) was identified as a replacement for TrimSol during milling of the equator weld-preps, however schedule and budget constraints prevented this change to occur. A picture of the dumb-bells and end-groups with half-cells for 5C75-003 prior to equatorial EB welding is shown in Fig. 8.

Figure 8. Dumb-bells and end-groups with end half-cells for 5C75-003 prior to machining the weld-preps on the dumb-bells' equators, cleaning and EB welding..

Two dumb-bells were sequentially EB welded to one end half-cell of a cavity from the inside and outside and the same was done with two other dumb-bells, EB welded to the other end half-cell. A picture of two dumb-bells welded to the end half-cell of 5C75-002 is shown in Fig. 9. A final full-penetration EB welding from the outside between two sub-assemblies was done to complete the cavity fabrication. The equator weld shrinkage was measured to be ~0.030" per weld, rather than 0.018" initially estimated. This is due to the inside/outside EB welding, each at a current of 35 mA. The larger than expected weld shrinkage was accounted for during machining of the dumb-bells for 5C75-001, as they were done after 5C75-002 and 5C75-003 were already completed. The higher weld shrinkage resulted in higher frequencies for 5C75-002 and 5C75-003. The frequency and field flatness of the cavities after fabrication are listed in Table IV and a picture of 5C75-003 is shown in Fig. 10. The following issues were reported during the equatorial EB welding:

- some inside welds required local required local re-welds - seemed to be prone to the "roll away" similar to a previously welded joint having the tendency to not flow or fuse
- a blow-through hole in cell 4 (from the FPC side) during the outer weld had to be repaired in 5C75-001
- significant weld splatter occurred during outer welding of cell 4 in 5C75-002

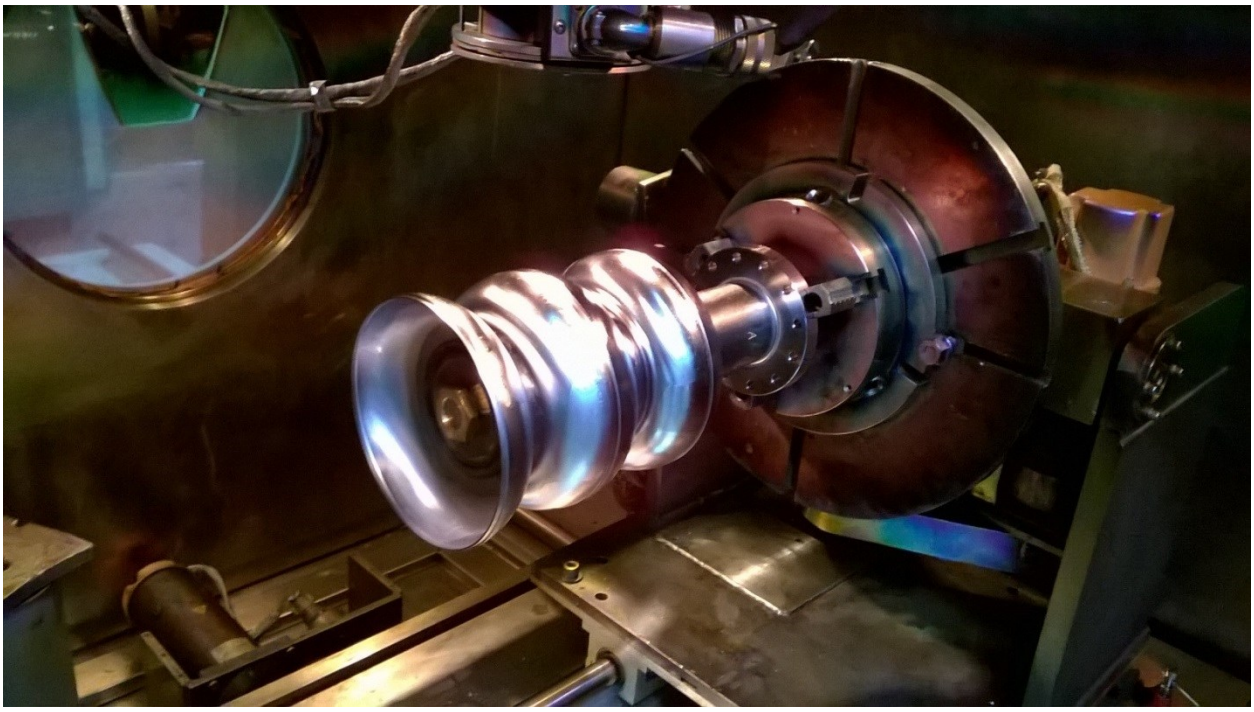

Figure 9. Picture of a subassembly of cavity 5C75-002 in the EB machine.

Figure 10. Picture of the fully welded 5C75-003 cavity.

Table IV. Frequency and field flatness of the three prototype cavities as fabricated.

Cavity	Frequency (MHz)	Field flatness
5C75-001	1495.619	77%
5C75-002	1496.703	86%
5C75-003	1497.236	85%

4. Cavity Processing and Testing

a. 5C75-001 and 5C75-002

After fabrication the cavities were tuned to a field flatness >90%. 5C75-001 and 5C75-002 were CBPed in three steps: in the first one, 4 h long, KM ceramic angle cut triangles (3/8"x3/8" 22°) were used as abrasive media. For the second step, RG-22 cones were used as abrasive media and the duration was 25 h, half of the time with the mandrel rotating in one direction and half with the mandrel rotating in the opposite direction. The last step was done using MF-3 treated corn cobs as polishing media, which resulted in a mirror finish surface. This step took 24 h and the rotating direction changed half-way through the CBP. The mandrel rotating speed was 115 rpm in all cases. After the first and second steps, the cavity was pressure washed and degreased in an ultrasonic tank with DI water and a detergent. The average material removal was 70 μm for each cavity, measured at four marked locations at the equator of each cell with an ultrasonic thickness measurement probe. Figure 11 shows a picture of a bare C75 cavity in the CBP machine.

Figure 11. Picture of one of the C75 cavities in the barrel in the CBP machine.

After CBP, the beam tubes were cut by wire EDM, ~0.020" was milled out from the cut surfaces, the machined surface were etched and the end-groups were EB welded from both inside and outside. Finally, the stiffening rings were welded between the waveguide walls and the end-cell wall.

A list of the processing steps for each cavity leading to the first RF test is given in Table V. The average material removal was measured with an ultrasonic thickness probe at the same locations of each cavity cell. In preparation for the vertical tests, the cavities were assembled in an ISO 5 clean room as follows:

- a stainless steel flange having an RF feedthrough with an antenna to couple power into the cavity and a pump-out port was attached to the cavity flange on the HOM waveguide side
- a Nb flange with an RF feedthrough with an antenna to probe the stored energy in the cavity was attached to the cavity flange on the FPC side
- After slow-pumpdown on a test stand and leak check, oscillating superleak transducers (OSTs) were attached to the cavity cage to detect quench locations and flux-gate magnetometers were attached to the cavity to measure the residual magnetic field in the dewar during cooldown

Table V. List of processing steps of cavities 5C75-001 and 5C75-002 after the end-groups were EB welded.

5C75-001	**5C75-002**
30 μm EP	35 μm EP
800 °C/ 3 h vacuum anneal	800 °C/ 3 h vacuum anneal
30 μm EP	20 μm EP
HPR	HPR

The RF test results at 2.07 K for cavities 5C75-001 and 5C75-002 are shown in Fig. 11. 5C75-001 quenched at 19.8 MV/m with a quality factor of 1.5×10^{10}, without field emission. 5C75-002 quenched at 11 MV/m with a quality factor of 9.6×10^{9}, without field emission. In both cases, the residual field in the dewar was ~5 mG during cool-down across T_c. The quench location was near the equatorial EB weld in cell 4 (from the FPC end group) for both cavities. An optical inspection of the cavities' inner surface near

the quench location showed the presence of defects, clearly associated to the equatorial EB weld in the case of 5C75-002, as shown in Fig. 13. Additional images of weld defects found in both cavities are shown in the Appendix.

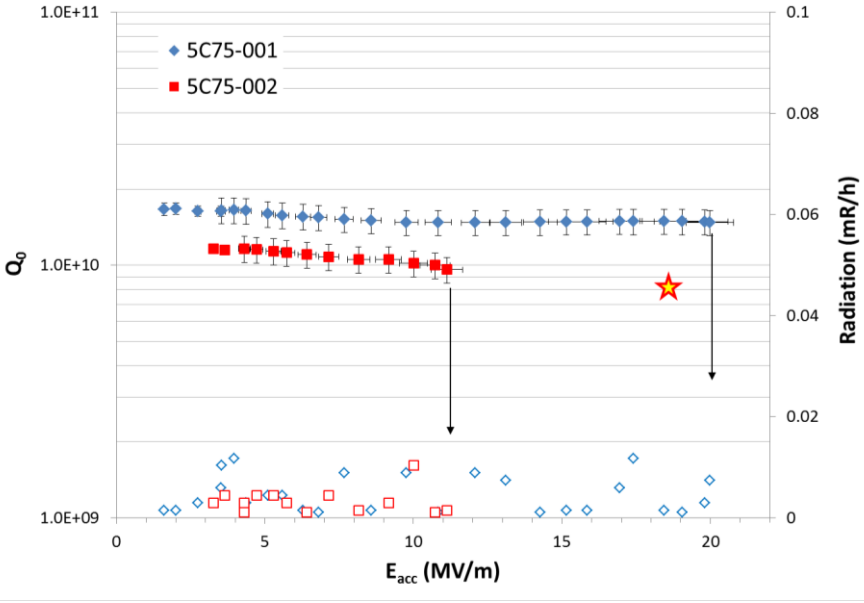

Figure 12. $Q_0(E_{acc})$ (solid symbols) and radiation dose rate vs. E_{acc} (empty symbols) measured at 2.07 K for 5C75-001 and 5C75-002. The "star" symbol is the performance specification for the C75 cavities.

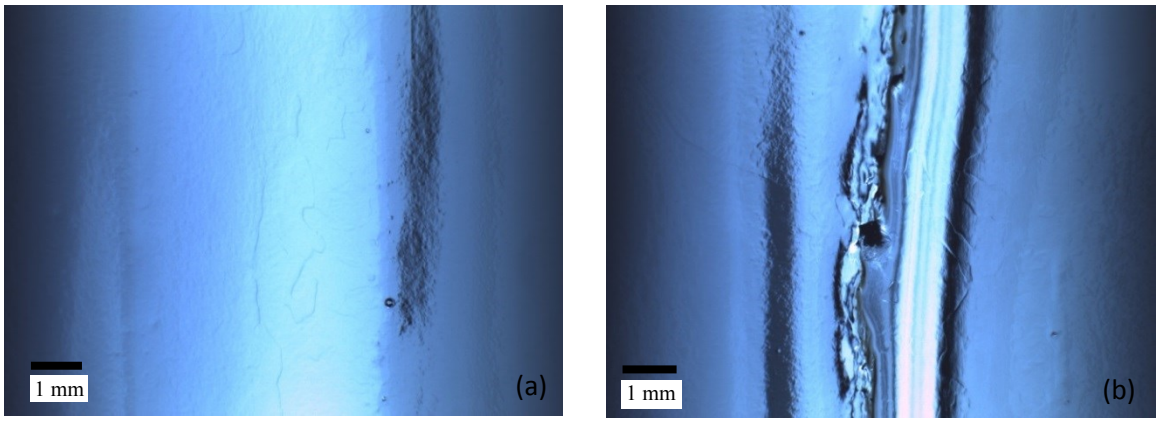

Figure 13. Defects found at the quench locations at the equator welds of cell 4 of cavities 5C75-001 (a) and 5C75-002 (b). The smoothening of the weld by CBP is clearly noticeable in (a).

b. 5C75-003

5C75-003 was tuned to >90% field flatness, etched by BCP 1:1:2 removing ~95 µm, annealed in vacuum at 600 °C for 10 h, electropolished to remove ~30 µm, degreased and high-pressure rinsed. The assembly, evacuation and cooldown procedures were the same as those of 5C75-001 and 5C75-002. For all C75 cavities, the cell temperature during EP was kept between 18-22 °C and the cathode voltage at 13 V. A plot of the parameters during EP of 5C75-003 is shown in Fig. 14. The results from all the RF tests

of 5C75-003 at 2.07 K are shown in Fig. 15. The first RF test was limited by early field emission and RF cable breakdown at 9 MV/m. The cavity was disassembled, re-HPRed, assembled, evacuated, leak checked, and cooled-down in a ~3 mG residual field. The second RF test was limited by quench at 15.6 MV/m with Q_0=7.8×10^9, without field emission. The quench occurred at the equator EB weld of cell 4. Optical inspection of the inner cavity surface after warm-up and disassembly showed large (~200 μm size) craters at the edge of the weld, as shown in Fig. 16. An attempt to repair the defects was made by local grinding using Cratex Al_2O_3 abrasive cylinders in three steps, with coarse, medium and fine grit. The defects were quite deep and it was not possible to completely remove them. After local grinding, the cavity inner surface was etched by BCP 1:1:2 removing ~30 μm followed by HPR, drying, assembly, evacuation. The results from the third RF test indicated a quench at 15.9 MV/m with a Q_0 of 7.8×10^9 and some field emission. This time, the cavity quenched in cell 5, near the equatorial EB weld. Optical inspection showed significant roughness of the weld area and a "surface relief" ~9 mm away from the weld, as shown in Fig. 16. Furthermore, severe pitting could be seen in cells 4 and 5, beyond ~2 cm on both sides of the equator weld and some stains surrounding the pits (an example shown in Fig. 18), which could indicate insufficient rinsing of the cavity after BCP.

A summary of the RF test results for all three cavities is given in Table VI.

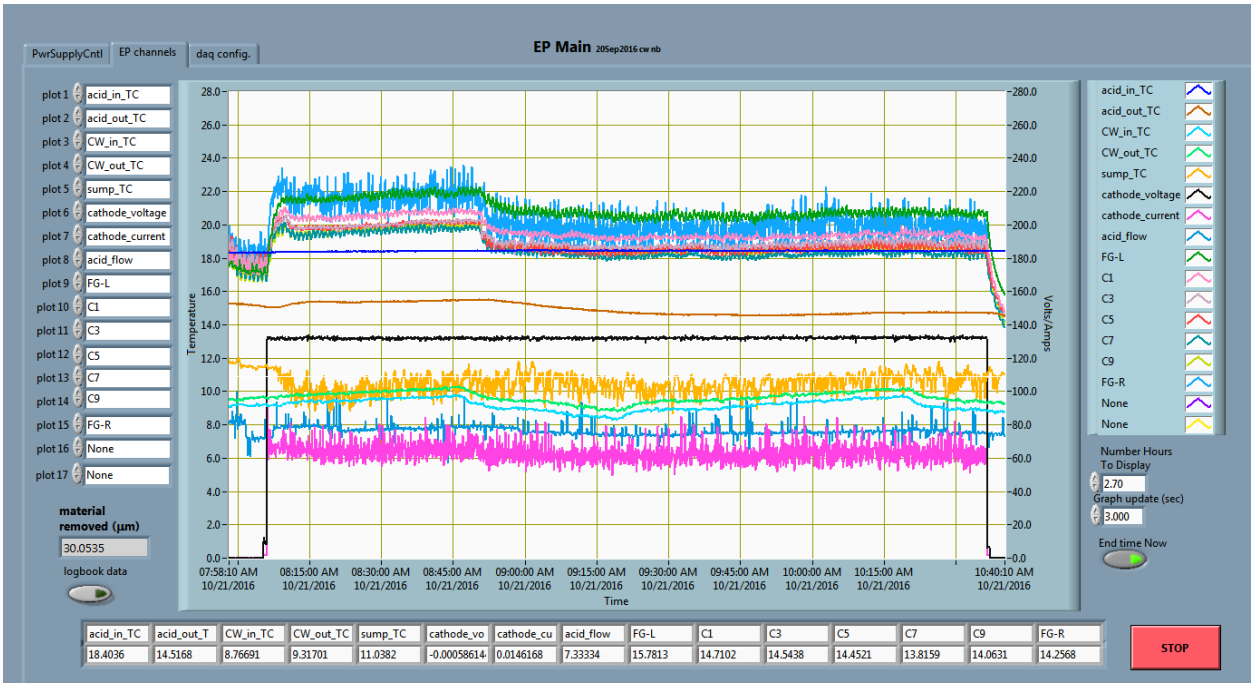

Figure 14. Plot showing temperatures at the equators, acid inlet and outlet, acid flow, cathode voltage and current during EP of C75-003.

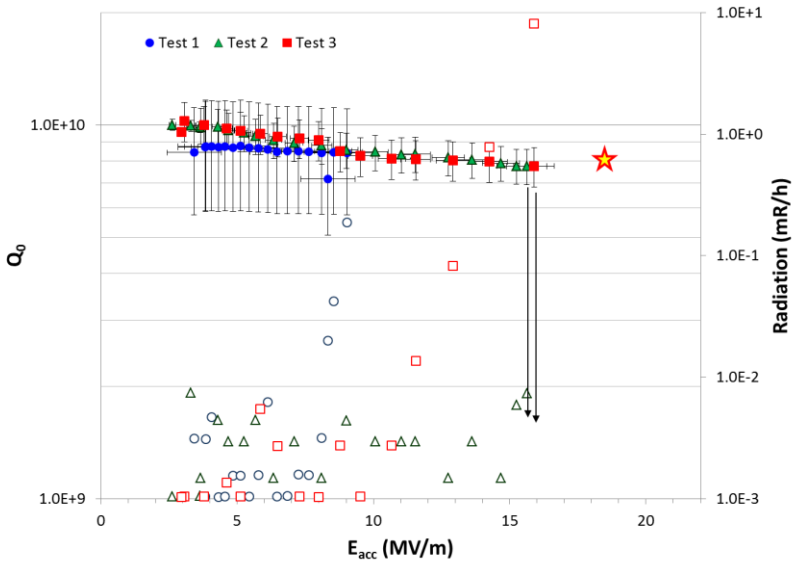

Figure 15. $Q_0(E_{acc})$ (solid symbols) and dose rate vs. E_{acc} (empty symbols) measured at 2.07 K for three tests on 5C75-003. The "star" symbol is the performance specification for the C75 cavities.

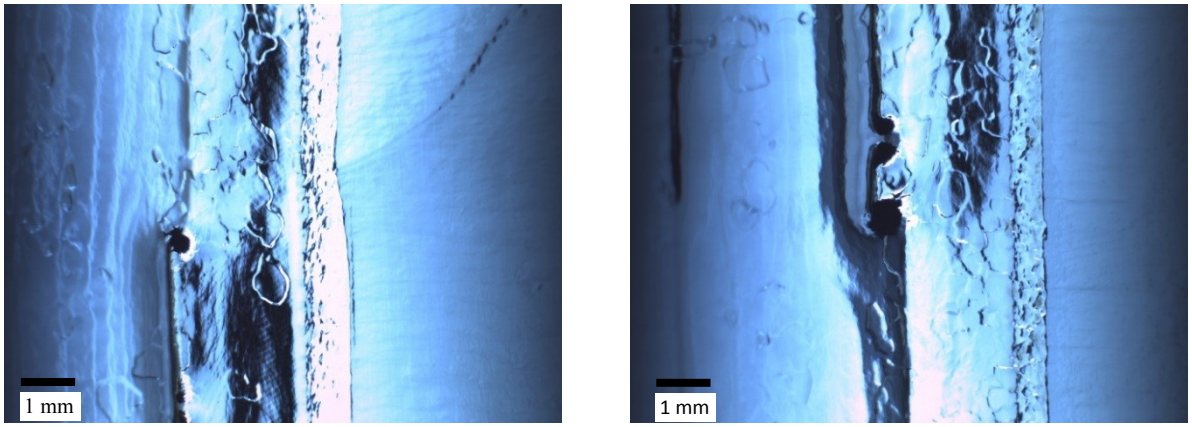

Figure 16. Defects found at the quench location at the equator weld of cell 4 of cavity 5C75-003 after test No. 2.

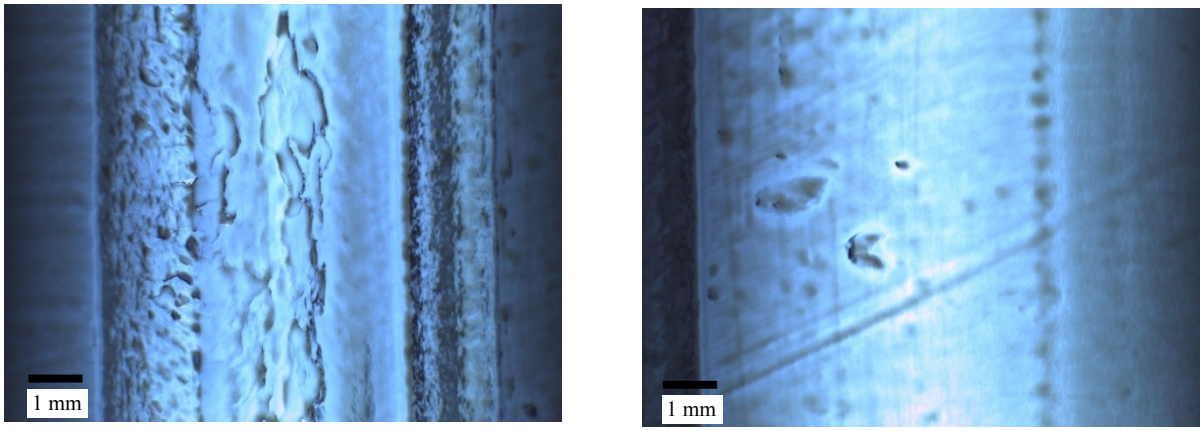

Figure 17. Protrusions on the weld (left) and ~9 mm from equator weld (right) in cell 5 near quench location of 5C75-003 after test No. 3.

Table VI. Summary of RF test results of C75 prototype cavities.

	5C75-001	**5C75-002**	**5C75-003**
Δf from 300 K, 1 atm to 2.07 K, 10^{-7} mbar (kHz)	2783	2780	2788
$\Delta f/\Delta P$ (Hz/Torr)	-185	-178	-196
$E_{acc,max}$ (MV/m)	19.8	11	15.9
$Q_0(E_{acc,max}$, 2.07 K)	1.5×10^{10}	9.6×10^{9}	7.8×10^{9}
R_{res} (nΩ)	0.3 ± 1	4.7 ± 0.2	3.8 ± 0.5

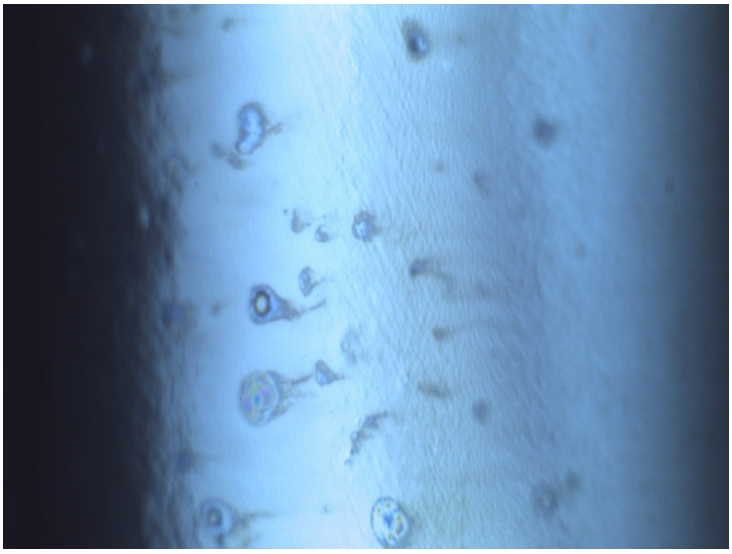

Figure 18. Example of pits surrounded by stains found at ~25 mm from the equator weld in several cells 5C75-003 after test No. 3.

c. 5C75-003 and 5C75-001 cavity pair

5C75-003 and 5C75-001 were prepared to be assembled into a cavity-pair for installation in cryomodule C50-7B (aka C50-13). The initial steps involved tuning to the room temperature target frequency of 1494. 520 MHz (±50 kHz) with >95% field flatness, tuning the FPC waveguide to achieve a Q_{ext} of $(2 \pm 1)\times10^7$ and measurements of cavity dimensions with a coordinate measuring machine. These operations had to be repeated a few times since straightening of some of the flanges was needed. The frequency at 300 K, 1 atm after final tuning was 1494.562 for 5C75-001 and 1494.566 for 5C75-003 and the Q_{ext} of the FPC was 2.2×10^7 for 5C75-001 and 1.8×10^7 for 5C75-003. Final polishing of flange surfaces was done afterwards, followed by a light etch of the flange's surfaces by BCP. The only surface treatment done to the inner surface of 5C75-001 was degreasing and HPR, whereas 5C75-003 received an additional ~20 μm EP to remove the acid stains shown in Fig. 18 and to attempt smoothing the pits. The cavity was then degrease and HPRed.

For cavity pair testing - unlike for the vertical test as single cavities - a Nb "dog-leg", a ceramic window and a Nb "top-hat" are assembled onto the FPC port of the cavity and Nb elbows with HOM loads are assembled to both HOM waveguide ports of each cavity. RF power is coupled into each cavity

with an antenna in the top-hat and the field probe is located in a port on one of the HOM waveguides. The cavity pair was cooled down in a residual magnetic field of less than 5 mG. The results of the RF tests at 2.07 K are shown in Fig. 19. 5C75-001 quenched at 19.3 MV/m with a Q_0 of 9.3×10^9 with a field emission onset of 17.3 MV/m, whereas 5C75-003 quenched at 13.7 MV/m with a Q_0 of 8.1×10^9 with a field emission onset of 9.9 MV/m. The results from the test of 5C75-001 show a decrease of Q_0 by ~50% compared to the results from the single-cavity test. Similar drop in Q_0-value was measured on an original CEBAF cavity (IA366) after the dog-leg, ceramic window and top-hat were installed and seem to indicate additional RF losses from the brazed joint between the window and the stainless steel flange. This issue needs to be further investigated in order to achieve lower RF losses in the cryomodule. Another issue, which limits the quality factor of cavities in original CEBAF cryomodules, is high residual magnetic field. This aspect is being address by adding a new magnetic shield around the cavities. The accelerating mode frequency at 2.07 K was 1497.368 MHz and 1497.435 MHz for 5C75-001 and 5C75-003, respectively.

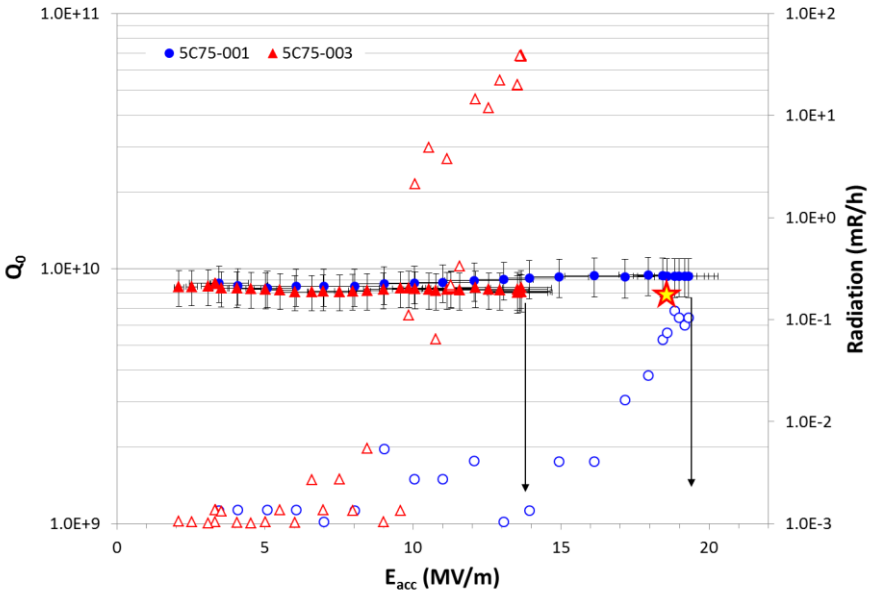

Figure 19. $Q_0(E_{acc})$ (solid symbols) and dose rate vs. E_{acc} (empty symbols) measured at 2.07 K for 5C75-001 (Nb RRR~120) and 5C75-003 (Nb RRR ~500) assembled into a cavity pair with dog-leg, RF window and top-hat. The "star" symbol is the performance specification for the C75 cavities.

In preparation of the vertical high power RF cavity pair test, loaded Qs of HOMs have been measured with a Vector Network Analyzer at 4 K temperature. The measurements were performed to check whether the most crucial dipole modes satisfy the beam break-up (BBU) impedance instability threshold for the CEBAF 12 GeV baseline machine operation (2.4×10^{10} Ohm/m) [8]. Note that such HOM measurements are generally not carried out for refurbished C50 cavity pairs since the HOM-damping is known to be better than in C100 Low Loss (LL) upgrade cavities. This is due to the fact that the original CEBAF (OC) cavities have only five instead of seven cells and that the aperture is comparably large (yields strong cell-to-cell coupling). This results in a stronger coupling of RF fields to the beam tubes when compared to the LL upgrade cavities, thus in a better damping capability by the HOM endgroup. An OC cavity HOM endgroup consists of two rectangular waveguides (TE10 cutoff is 1.9 GHz). The HOM

waveguides are terminated with loads that can dissipate RF energy over a broad spectrum at the operating temperature (2 K). However, the OC cavities have to also rely on HOM damping through the FPC (TE10 cutoff is 1.1 GHz) for some modes of the TE111 passband, which resonate below 1.9 GHz and would be otherwise trapped in the cavity. As conceived originally, this requires an HOM filter in each power transmission line for the old CEBAF cryomodules. The HOM filters are installed outside the cryomodule and can absorb the RF energy traveling towards the klystron, while designed with a small insertion loss for the fundamental waveguide mode fed into the cavity.

One complication for the characterization of HOMs in the vertical dewar is that the assembly (dog-leg, ceramic window and top-hat) attached to the cavity FPC port does not provide a sufficiently broadband absorbing condition. Consequently, the lower frequency TE111 modes cannot be adequately damped as it would be the case in a cryomodule. Corresponding Q-values are overestimated. Moreover, we have not been able to find any documentation of Q-values for OC cavities measured in the vertical dewar. Such measurements could serve as a reference, i.e. which Q-values one may expect for the trapped TE111 modes before cryomodule string installation. Therefore we rely on numerical findings that have been carried out for OC or C75 cavities with or without damping through the FPC. The simulations revealed that one can expect external Q-values within 1×10^{8}-1×10^{9} for some of the trapped TE111 modes if the damping through the FPC is not taken into account. This also depends on the mode polarization since the damping through the FPC (pointing in horizontal direction) is most efficient for horizontally polarized TE111 modes.

The impedance of each HOM was evaluated utilizing the product of the simulated R/Q-value and the measured Q-values ($R/Q_{sim} \times Q_{meas}$). The corresponding results for the C75 cavity pair are shown in Fig. 20 comprising the most crucial TE111 and TM110 dipole passbands. Uncertainties remain concerning mode identification as not all existing HOMs could be detected with the used antennas probes. Furthermore, HOM frequencies varied among the two cavities depending on fabrication tolerances and deviations exceeding 10 MHz compared to simulations for the ideal shape are observed. Overall, the results demonstrate that the impedance threshold for BBU (dashed line) is not exceeded even for the trapped TE111 modes, which are not properly damped in the vertical assembly. The highest Q-value measured was 4×10^{7} for a TE111 mode part of the first dipole pair resonating at 1.74 GHz.

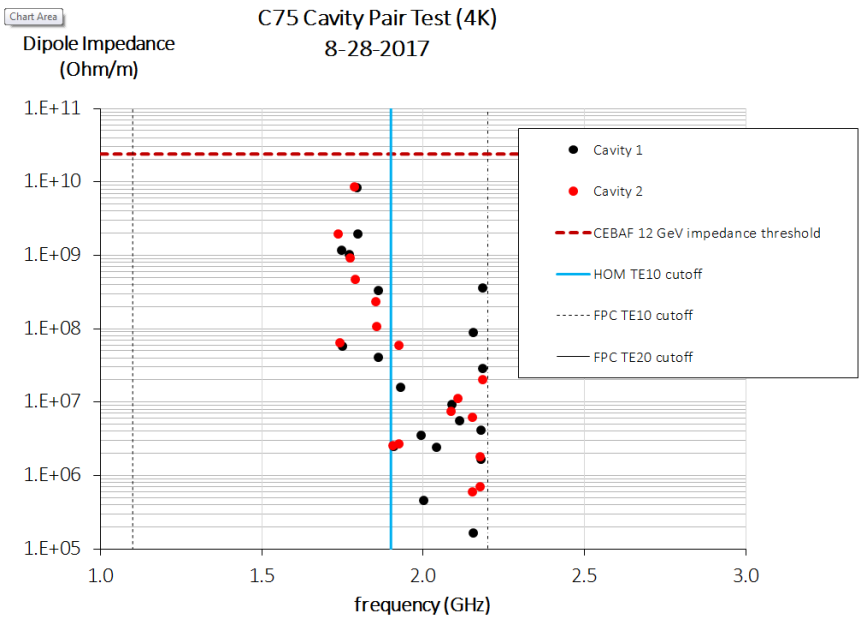

Figure 20. TE111 and TM1110 dipole impedances for 5C75-001 and 5C75-003 assembled into a cavity pair with dog-leg, RF window and top-hat. The highest dipole impedance (close to 1×10^{10} Ohm/m) is a rather conservative estimate multiplying a relatively high Q-value measured (1.8×10^{6} at 1.79 GHz) with the largest dipole R/Q-value closest to that frequency as simulated (4842 Ohm/m at 1.80 GHz). The unit Ohm/m reflects the normalization of the longitudinal impedance evaluated at radial offset *r* from the axis (depending on mode polarization) by $k\cdot r^2$ with *k* denoting the wave number of the HOM.

It shall be noted that the FPC for C75 cavities yields a higher Q_{ext}-value (2×10^{7}) by design when compared to the original value ($Q_{ext} = 6.6\times10^{6}$) for OC cavities. This provides a better match of the generator power for the CEBAF 12 GeV beam operation considering maximum beam loading and 32 Hz peak microphonics as a realistic estimate. In order to increase the Q_{ext}-value, while reusing existing OC cavity FPC waveguides, the C75 cavity FPC port had to be positioned further away from the end cell iris by several millimeters, which comes in tradeoff with the HOM damping through the FPC.

5. Discussion

Equatorial EB welds are one of the most critical aspects of the fabrication of SRF cavities which impact the gradient performance. Historically, weld issues have limited the ultimate field of multi-cell cavities made of ingot Nb material at JLab. On the other hand, industry was capable to produce eleven 1.3 GHz, 9-cell cavities, which reproducibly achieved $E_{acc} > 35$ MV/m with standard EP treatment [9]. In spite of changes made for the fabrication of the C75 prototype cavities to improve the reliability of the welds, repairs were still necessary and several defects were seen at the welds by optical inspection.

Comparing some of the cavity fabrication techniques between industry and at JLab, several important differences exist:

- the weld prep is machined on the equator dumb-bell on a lathe with tools dedicated to only machine Nb, rather than by milling

- The weld prep is an interlocking “step-joint”, rather than a “butt-joint”

These two aspects can be important especially when fabricating cavities from ingot material, for which maintaining the roundness of the equator is more challenging. Misalignment of parts with a “butt-joint” could easily occur along the equator circumference, as it is indicated by some of the images in the Appendix, and result in welds with defects or sharp edges. Furthermore, dedicated lathe and tooling to only machine Nb parts are used in industry to reduce chances for contamination of the parts with foreign materials.

In addition, the controls and the camera system of the EB welding machine at JLab are outdated and is often difficult for the operator to actually see the joint and to judge the quality of a weld. Issues during welding of Nb fine-grain cavity parts for a project which followed the C75 prototypes required intervention of a maintenance technician from the company who had originally built the EB welding machine and faulty components and settings needed to be fixed. This suggests the need for an annual maintenance period in which the whole EB machine is checked.

6. Conclusion

Three prototype ingot Nb cavities for boosting the energy gain of CEBAF refurbished cryomodules were built, processed and tested at JLab. The performance specifications were not achieved in two of the cavities because of issues during fabrication. The two best cavities will be installed in the next C50 cryomodule to be commissioned in CEBAF in Summer 2017. Improvements in the cavity fabrication techniques and in the EB welding machine at JLab are necessary to allow reliably achieving the gradient specification, if more cavities were to be built “in house”. Additional RF losses by the FPC window also need to be further understood and mitigated in order to reliably achieve the quality factor specification. Additional RF losses due to high residual magnetic field are being addressed by adding a new magnetic shield close to the cavities.

7. References

[1] H. Wang, R. Rimmer and G. Wu, “Elliptical Cavity Shape Optimization for Acceleration and HOM Damping”, Proc. PAC’05, Knoxville, TN, 2005, p. 4191.

[2] P. Kneisel *et al*., *Nucl. Inst. Meth. Phys. Res. A* **774** (2015) 133–150

[3] G. Ciovati, P. Dhakal and G. R. Myneni, *Supercond. Sci. Technol*. **29** (2016) 064002.

[4] P. Kneisel, “Progress on large grain and single grain niobium - ingots and sheet and review of progress on large grain and single grain niobium cavities”, Proc. SRF’07, Beijing, China, 2007, p. 728.

[5] G. Ciovati et al., “Tuning sensitivity and stiffness of C20/C50 and C75 cavities”, Jefferson Lab Technical Note TN-17-017, 2017.

[6] G. Ciovati, P. Kneisel and G. R. Myneni, “America’s overview of superconducting science and technology of ingot niobium”, in *Proc. of the Symposium on the Supercond. Sci. and Technol. of Ingot Niobium*, AIP Conf. Proc. **1352**, 2011, p. 25.

[7] R. Geng and O. Trofimova, “Characterization and Control of Foreign Materials on Post-Machined Niobium Surface”, presented at the 2014 TTC Meeting, Tsukuba, Japan, Dec. 2-5, 2014.

[8] J. Guo and H. Wang, *Physics Procedia* **79** (2015) 30-37.

[9] W. Singer *et al*., *Phys. Rev. ST Accel. Beams* **16** (2013) 012003.

8. Appendix

Additional images of EB weld defects found by optical inspection of C75 prototype cavities after RF testing are shown in the following figures.

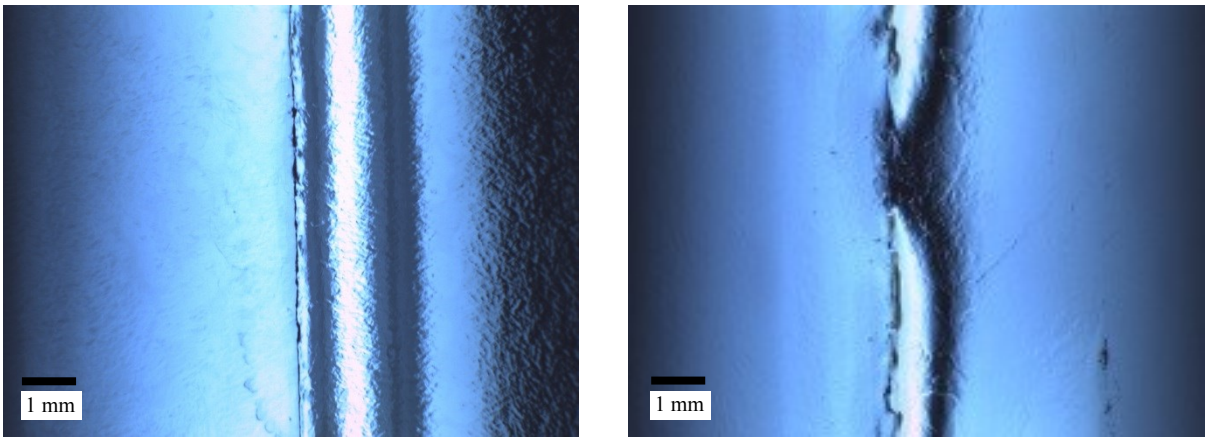

Figure A1. Image of the inner surface of areas of the equator weld of cells 1 (left) and 4 (right) in cavity 5C75-002 showing a sharp line between the weld and the surrounding Nb and a non-uniform weld, respectively.

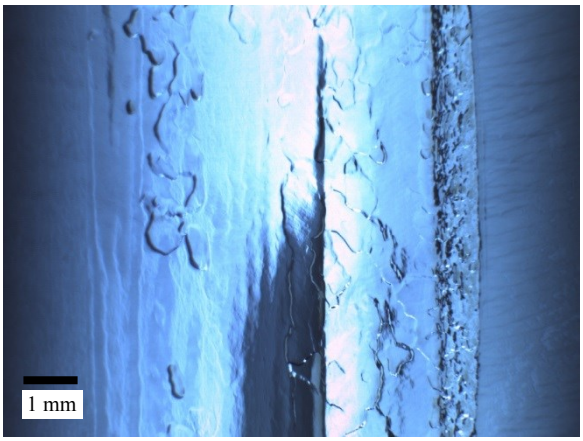

Figure A2. Images of the inner surface of an area of the equator weld area of cell 4 in cavity 5C75-003 showing a ridge.

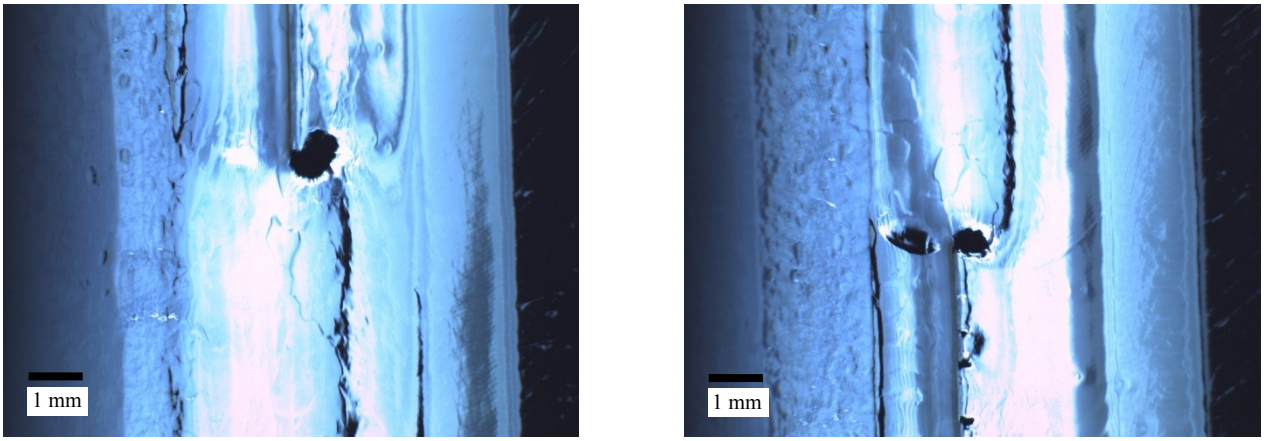

Figure A3. Images of two sections of the equator weld of cell 4 in cavity 5C75-003 showing craters and a partial re-weld at an offset.